

Model of the Electronic Structure of Electron-Doped Iron-Based Superconductors: Evidence for Enhanced Spin Fluctuations by Diagonal Electron Hopping

Katsuhiro Suzuki¹, Hidetomo Usui¹, Soshi Iimura², Yoshiyasu Sato²,
Satoru Matsuishi³, Hideo Hosono^{2,4}, and Kazuhiko Kuroki¹

¹ *Department of Physics, Osaka University, Toyonaka, Osaka 560-0043, Japan*

² *Materials and Structures Laboratory, Tokyo Institute of Technology, Yokohama 226-8503, Japan*

³ *Materials Research Center for Element Strategy,*

Tokyo Institute of Technology, Yokohama 226-8503, Japan and

⁴ *Frontier Research Center, Tokyo Institute of Technology, Yokohama 226-8503, Japan*

(Dated: November 6, 2018)

We present a theoretical understanding of the superconducting phase diagram of the electron-doped iron pnictides. We show that, besides the Fermi surface nesting, a peculiar motion of electrons, where the next nearest neighbor (diagonal) hoppings between iron sites dominate over the nearest neighbor ones, plays an important role in the enhancement of the spin fluctuation and thus superconductivity. In the highest T_c materials, the crossover between the Fermi surface nesting and this “prioritized diagonal motion” regime occurs smoothly with doping, while in relatively low T_c materials, the two regimes are separated and therefore results in a double dome T_c phase diagram.

In theoretical studies of high T_c superconductors, one of the most important challenges is to extract the minimal essence of the material that leads to the strong pairing state. After the discovery of the iron-based superconductors[1], the nesting between electron and hole Fermi surfaces has been considered as such an essential feature, and therefore, the identity of the family. In fact, several theoretical studies suggested a possibility of spin fluctuation mediated pairing, where the spin fluctuation arises around the nesting vector $(\pi, 0)$ [2–9]. The spin fluctuation mediates $s\pm$ -wave pairing, where the gap function has s -wave symmetry, but its sign is reversed between the electron and hole Fermi surfaces.

However, recent experiments suggest that high T_c is obtained when the nesting is degraded, or even in the absence of the nesting[10–14]. Then, a question of great interest is “what is the key ingredient for high T_c *peculiar to the iron-based superconductors*?” In this context, the so-called hydrogen-doped 1111 systems, $LnFeAsO_{1-x}H_x$ ($Ln = \text{Gd, Sm, Ce, La}$)[14] where a large amount of electrons can be doped by $O \rightarrow H$ substitution, provide us with some important clues. For $Ln = \text{La}$, the T_c vs x (doping rate) phase diagram exhibits a double dome feature, and the second dome has higher T_c than the first (see Fig. 2). The normal state properties above T_c such as the temperature dependence of the resistivity are also different between the two domes. On the other hand, for $Ln = \text{Sm, Ce, Gd}$, the phase diagram exhibits a single dome feature, and very high T_c ’s close to or exceeding 50 K are observed. These single dome materials share commonalities with the second T_c dome of $\text{LaFeAsO}_{1-x}\text{H}_x$ [14], so that understanding the origin of the second dome directly leads to the origin of the very high T_c in the iron-based superconductors.

One can easily expect that the Fermi surface nesting is degraded in the second dome compared to that in the first due to the large amount of doped electrons. In fact, the

present study reveals that while the first T_c dome originates from the spin fluctuation induced by the nesting of the Fermi surface having $d_{xz/yz}$ (and also d_{xy} in some cases) orbital components, the second T_c dome is due to the spin fluctuation enhanced by a peculiar motion of electrons within the d_{xy} , where the second neighbor diagonal hoppings are larger than the nearest neighbor ones. Such an electron motion is specific to the tetrahedral coordination of the pnictogen atoms, and we conclude that this prioritized diagonal motion is a key factor giving rise to the high T_c . In the single dome T_c materials, “the nesting dominating” and the “prioritized diagonal motion” regimes are not well separated, and the highest $T_c \sim 50\text{K}$ is attained around the crossover regime. Then, another important key ingredient for high T_c is that the d_{xy} and $d_{xz/yz}$ orbitals both act as driving forces of the same pairing state, namely, $s\pm$ -wave pairing. Among various multiorbital systems, this is an unparalleled feature peculiar to the iron-based superconductors.

In 1111 systems, electrons are doped into the FeAs layer by substituting O^{2-} with F^- or H^- . The doping actually affects the electronic band structure in two ways; i.e., the increase of positive and negative charges in the $Ln\text{O}$ and FeAs layers, respectively, and the reduction of the As-Fe-As bond angle. The bond angle reduction occurs linearly with doping as shown in Fig.S1 of the Supplemental Material[15]. Changing the rare earth element appears as a parallel shift of the bond angle variance against the doping rate. Quite recently, this trend has further been confirmed by partially replacing As by P in $\text{SmFeAsO}_{1-x}\text{H}_x$ [22], where a double dome phase diagram is found for sufficient amount of phosphorous substitution. To model these effects, band structure calculations are performed using the VASP code[23] for hypothetical variations of LaFeAsO , where we (i) adopt the virtual crystal approximation replacing the oxygen potential by a $1 - x : x$ mixture of oxygen and fluo-

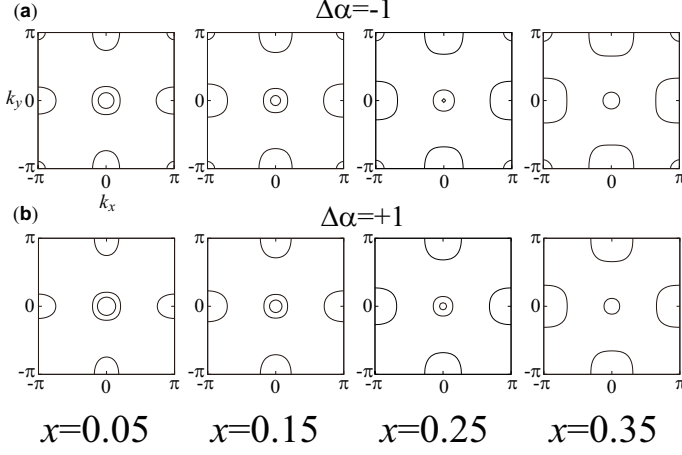


FIG. 1. Fermi surfaces for $x = 0.05$, $x = 0.15$, $x = 0.25$, $x = 0.35$ with (a) $\Delta\alpha = -1^\circ$ or (b) $\Delta\alpha = +1^\circ$.

rine potentials[14] ($x = 0.05 \sim 0.5$ with an increment of 0.05), and (ii) vary the bond angle linearly according to x as $\alpha(x) = -7.48x + 114.36 + \Delta\alpha$, where $\Delta\alpha$ is the amount of parallel shift made with respect to the actual bond angle variance of $\text{LaFeAsO}_{1-x}\text{H}_x$. We consider $\Delta\alpha = -3, -2, -1, 0, +1, +2^\circ$, as shown in Fig.S1 in the Supplemental Material[15]. Varying $\Delta\alpha$ corresponds to considering materials with different rare earth (Ln) or anion (As partially replaced by P) elements[24]. To capture the essence, we vary only the bond angle, while fixing the Fe-As bond length. By extracting the bands near the Fermi level using the Wannier90 package[25], we construct models consisting of d_{xy} , d_{yz} , d_{xz} , $d_{x^2-y^2}$, and $d_{3z^2-r^2}$ Wannier orbitals[3]. Considering that the three dimensionality is not essential to the single vs. double dome issue, we omit the interlayer hoppings, and concentrate on two dimensional models in which the Brillouin zone can be unfolded to obtain a five orbital model [3].

Figure 1 shows the Fermi surface evolution with doping for $\Delta\alpha = +1^\circ$ and -1° . The main difference between the two cases is the presence or absence of the Fermi surface around the wave vector (π, π) , which originates from the d_{xy} orbital[26]. The volume of the electron Fermi surfaces around $(\pi, 0)$ and $(0, \pi)$ increases with doping, and the hole Fermi surfaces around $(0, 0)$, arising from the d_{xz}/d_{yz} orbitals, shrink. On the other hand, The volume of the d_{xy} hole Fermi surface around (π, π) remains nearly unchanged due to the band structure variation with doping[27, 28]. In any case, the volume difference between electron and hole Fermi surfaces increases with doping, so that the nesting becomes ill-conditioned.

Considering intra- and interorbital electron-electron interactions on top of the five orbital band structure, we apply the fluctuation exchange (FLEX) approximation[6, 29, 30] to each model, and obtain the eigenvalue of the Eliashberg equation λ (at a fixed temperature of $T = 0.005\text{eV}$), which is taken as a measure of T_c . We

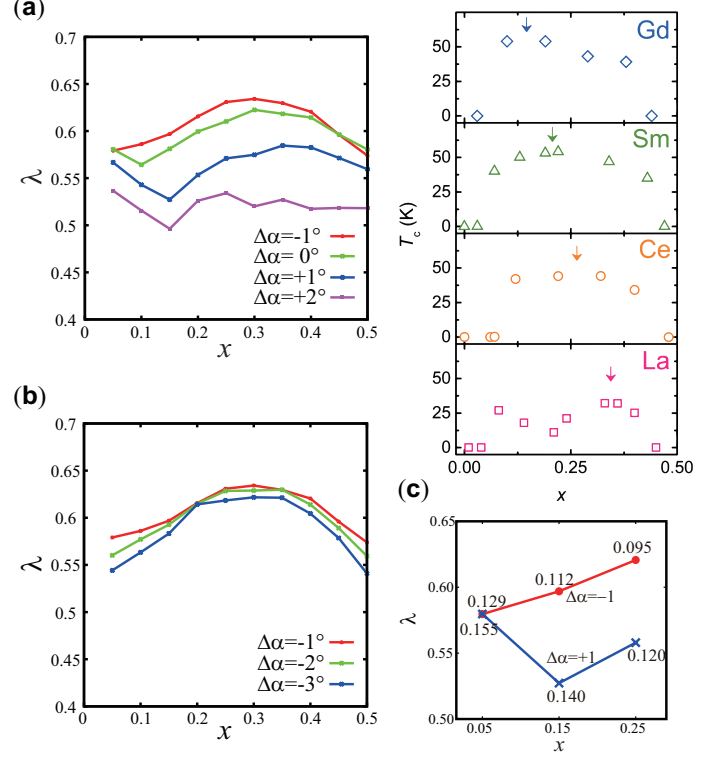


FIG. 2. Eigenvalue of the Eliashberg equation against doping. (a) λ against doping for $\Delta\alpha = -1, 0, +1, +2^\circ$. (b) Similar as in (a) for $\Delta\alpha = -3, -2, -1^\circ$. (c) λ for simplified models in which only t_1 is varied in conjunction with x so as to maintain the volume of the (π, π) Fermi surface. The numbers are the values of t_1 (in eV). Here, t_2 is fixed at 0.106 (0.113) eV for $\Delta\alpha = -1$ (+1). See text for more details. Upper right panel: Experimental result of T_c vs x for $Ln\text{FeAs}(\text{O},\text{H})$ with $Ln = \text{Gd}, \text{Sm}, \text{Ce}, \text{La}$ (from Ref. 14).

take intraorbital $U = 1.3\text{eV}$, the interorbital $U' = U - 2J$, Hund's coupling, and the pair hoppings $J = J' = U/6$. In a previous study, we adopted random phase approximation, where the self energy correction was neglected[28]. There, the eigenvalue of the Eliashberg equation was found to be monotonically enhanced with electron doping, which does not agree with the experimental observations. Also, the origin of the material dependence of the phase diagram was not clarified.

The calculated eigenvalues of the Eliashberg equation λ for $\Delta\alpha = -1^\circ \sim +2^\circ$ are shown in Fig. 2(a). For $\Delta\alpha = -1^\circ$, the λ against x plot shows a “single dome” variance. This is already quite interesting in that the magnitude of λ (and, hence, T_c) is maintained in such a large doping range. Even more interestingly, for $\Delta\alpha = 0^\circ$, there appears a slight dip in the lightly doped regime, and this feature becomes more pronounced for $\Delta\alpha = +1^\circ$ and $+2^\circ$. Also, the maximum T_c is obtained at a larger doping rate when $\Delta\alpha$ is increased. Similar results are obtained also for orbital dependent interactions (Supplemental Material[15] Fig. S3). In Fig. 2 (b), we

show the doping dependence of λ for $\alpha = -1^\circ \sim -3^\circ$. It can be seen that the increase of λ with x in the lightly doped regime becomes more rapid with decreasing $\Delta\alpha$. These results are overall in good agreement with the trend observed experimentally in Ref. 14 (Fig. 2, upper right panel) and also Ref. 24.

In Fig. 3, we show the doping dependence of the intraorbital spin susceptibility χ_{xy} and $\chi_{xz/yz}$ within the d_{xy} and d_{xz}/d_{yz} orbitals[31] for $\Delta\alpha = +1^\circ$ and -1° . Let us first focus on $\Delta\alpha = -1$. For $x = 0.05$, there appear peaks around $(\pi, 0)$ and $(0, \pi)$ in both χ_{xy} and $\chi_{xz/yz}$ reflecting the Fermi surface nesting in the lightly doped system.

These peak structures are suppressed by electron doping because the nesting is degraded. However, χ_{xy} is unexpectedly reenanced beyond $x \sim 0.2$. The reason for this cannot be the Fermi surface nesting in its original sense because the nesting is monotonically degraded by doping. For $\Delta\alpha = +1^\circ$, on the other hand, the variance of χ_{xy} is different in that there is no enhancement in the lightly doped regime. The absence of enhanced χ_{xy} there is natural because the d_{xy} hole Fermi surface around (π, π) is absent for $\Delta\alpha = +1^\circ$, so that there is no Fermi surface nesting. Conversely, it is surprising to find an enhancement in the largely doped regime. Interestingly, an inelastic neutron scattering experiment for $\text{LaFeAsO}_{1-x}\text{H}_x$ actually observes the suppression of the spin fluctuation around $x \sim 0.2$ and its reenancement in the largely doped regime[32]. Also, comparing $\Delta\alpha = -1^\circ$ and $\Delta\alpha = +1^\circ$, the spin fluctuation grows more rapidly with doping for the former than for the latter.

The doping dependence of the Eliashberg equation eigenvalue λ and the intraorbital spin fluctuations are strongly correlated, so that understanding the latter directly leads to the understanding of the former. Since the Fermi surface evolution does not seem to be correlated with the doping dependence of the spin fluctuation, we now focus on the real space hopping integrals within the d_{xy} orbitals. In Fig. 4, we plot the doping dependence of the nearest (t_1) and the next nearest (t_2) neighbor hoppings within the d_{xy} orbitals for $\Delta\alpha = -1^\circ$ and $+1^\circ$. The nearest neighbor hopping t_1 decreases rapidly with doping, and becomes smaller than t_2 at a certain doping rate $x_c \sim 0.17$ for $\Delta\alpha = -1^\circ$ and $x_c \sim 0.28$ for $\Delta\alpha = +1^\circ$. We also show in Fig. 4(b) the calculation result for the actual La1111 and Sm1111 using the experimentally determined lattice parameters. It is indeed seen that x_c is larger for La than for Sm corresponding to the larger bond angle in the former. We will refer to this peculiar hopping relation $t_2 > t_1$ as “prioritized” diagonal motion (or hopping) of electrons.

The rapid decrease of t_1 by doping as compared to t_2 can be understood as a combined effect of (i) the increased positive charge in the LaO layer, (ii) reduction of the Fe-Fe distance, and (iii) increase of the pnictogen height, where (ii) and (iii) are the effects of the bond

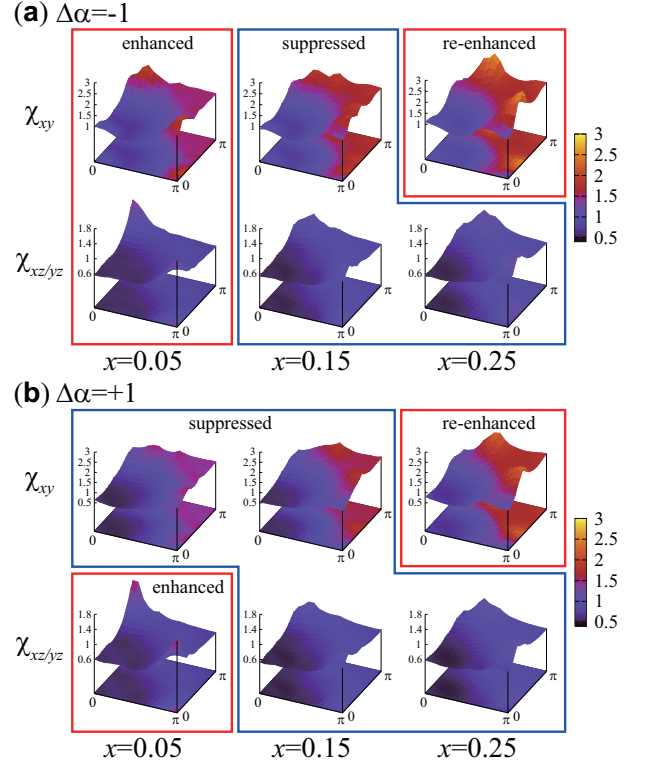


FIG. 3. Intraorbital spin susceptibilities χ_{xy} and $\chi_{xz/yz}$ for $x = 0.05, 0.15$, and 0.25 . (a) $\Delta\alpha = -1^\circ$ and (b) $\Delta\alpha = +1^\circ$.

angle reduction. In the five orbital model, we consider Wannier orbitals, which implicitly take into account the Fe $3d$ and the hybridized As $4p$ atomic orbitals. If we consider these atomic orbitals explicitly, the present t_1 can be expressed as $t_1 = t_1^{\text{direct}} + 2t_1^{\text{indirect}}$, where t_1^{direct} and t_1^{indirect} are contributions from the direct hopping between Fe $3d_{xy}$ orbitals and the indirect hopping via As $4p$, respectively, as shown in Fig. 4. The two contributions have opposite signs, and t_1^{indirect} dominates in the lightly doped regime. This cancellation of the direct and indirect hoppings has been discussed in Refs.[33, 34]. On the other hand, the next nearest neighbor t_2 is mainly governed by t_2^{indirect} because of the larger Fe-Fe distance. As electrons are doped, the energy level of the As $4p$ orbital is lowered and moves away from the Fe $3d$ level due to the effect of (i), so that the indirect hoppings decrease. The indirect contribution is also reduced because of (iii). By contrast, the direct hopping increases due to (ii). The combined effect of increasing t_1^{direct} and decreasing $|t_1^{\text{indirect}}|$ results in a rapid decrease of t_1 with doping. The effect is weak for t_2 because it is mainly dominated by t_2^{indirect} . As can be understood from this explanation, x_c is larger for materials with larger $\Delta\alpha$.

Intuitively, $t_1 < (>) t_2$ corresponds to $J_1 < (>) J_2$ in the limit of strong electron correlation[35, 36] since $J_i \propto t_i^2/U$, where U is the on-site intraorbital repulsion. Therefore, $t_1 < [> 0] t_2$ is naively expected to

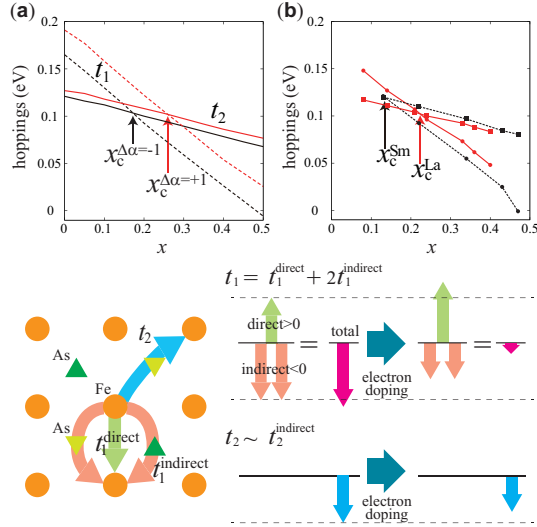


FIG. 4. Upper panels: doping dependence of the real space hopping integrals t_1 and t_2 against the doping. (a) $\Delta\alpha = +1^\circ$ (red or gray) and $\Delta\alpha = -1^\circ$ (black). Solid (dashed) lines are t_2 (t_1). (b) Actual materials La1111 (red or gray) and Sm1111 (black). Circles (boxes) are t_1 (t_2). Lower panels: schematic figure of the origin of the prioritized diagonal hopping with doping.

be in favor of the $(\pi, 0)$ [(π, π)] spin fluctuations. More precisely, however, the enhancement of the spin fluctuation in the largely doped regime should be traced back to the band structure (not just the Fermi surface) since we are adopting FLEX, which is essentially a weak coupling approach. In fact, as shown in the Supplemental Material[15] (Fig.S2), the shape of the band changes with doping, which is mainly due to the reduction of t_1 . The disappearance of the van Hove singularity around the wave vector $(\pi, 0)$ (reminiscent of those commonly seen in the cuprates) works in favor of the $(\pi, 0)/(0, \pi)$ spin fluctuations over (π, π) .

In the models adopted above, not only t_1 , but also other parameters vary with electron doping. To more directly single out the reduction of t_1 as the key factor, we have done the following analysis using simplified models. Namely, we start with five orbital models derived from a first principles band calculation performed with $\Delta\alpha = -1$ or $+1$, both with 15% fluorine doping. Within these models, we vary the electron density in the range of $0.05 \leq x \leq 0.25$. If all the hoppings were fixed (rigid band), the hole Fermi surface would monotonically shrink as x increases. As seen above, however, the Fermi surface around (π, π) is almost unchanged with electron doping if the variance of the lattice parameters and the O \rightarrow F substitution effect is taken into account in the first principles calculation. To simulate this effect, in the simplified models, we vary only t_1 by hand in conjunction with the electron doping so that the volume of the (π, π) Fermi surface is the same as that for the original model. For

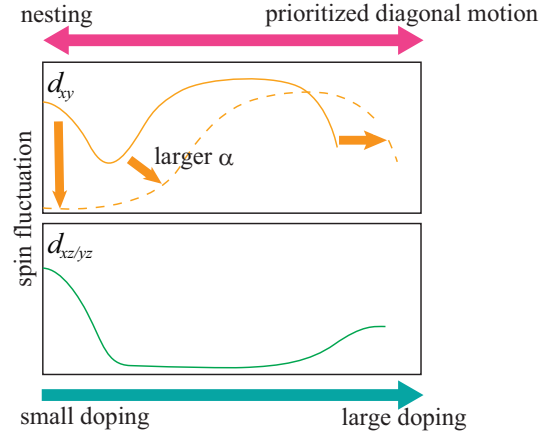


FIG. 5. Schematic figure of the spin fluctuation contribution to superconductivity.

$\Delta\alpha = +1$, where the (π, π) hole Fermi surface is absent, the energy difference between the chemical potential and the top of the d_{xy} band at (π, π) is kept to be the same as that in the original model. λ calculated this way as a function of x for $\Delta\alpha = \pm 1$ is shown in Fig. 2 (c), where a trend similar to that in Fig. 2 (a) is seen; when t_1 is significantly larger than t_2 , λ decreases with doping, while when t_1 is comparable to or smaller than t_2 , λ increases with doping.

In Fig. 5, we show a schematic figure of the spin fluctuation contribution to $s\pm$ superconductivity. For the d_{xz}/d_{yz} orbital, there is spin fluctuation mediated pairing arising from good nesting in the lightly doped regime, which is suppressed by doping because the nesting is degraded. In the d_{xy} orbital, there can be moderate Fermi surface nesting in the lightly doped regime depending on the absence or presence of the d_{xy} hole Fermi surface around (π, π) . Therefore, for materials with small (i.e., negative) $\Delta\alpha$, the d_{xy} spin fluctuation crosses over from the nesting to the prioritized diagonal motion regime. On the other hand, in materials with large (positive) $\Delta\alpha$, there is no nesting regime in the d_{xy} orbital, so that the d_{xy} spin fluctuation monotonically increases with doping. For materials with small bond angle, the crossover from the nesting to the prioritized diagonal motion regime occurs smoothly because x_c is small. Therefore, the T_c phase diagram consists of a single dome. x_c is large for materials with large bond angle, so that the two regimes are separated, resulting in a double dome structure of the phase diagram. Interestingly, we have also come to realize a relation between the spin fluctuation and the resistivity, which is explained in the Supplemental Material[15] (Fig.S4).

To conclude, our study has revealed the importance of the peculiar motion of electrons in the d_{xy} orbital, especially in cases with very high T_c . Further tests for the present conclusion can be performed by examining the pressure effect. In Ref.[14], it was found that apply-

ing pressure to LaFeAs(O,H) makes the double dome T_c phase diagram turn into a single dome one. Our preliminary theoretical study on this problem shows that applying pressure enhances the t_2/t_1 ratio, and hence has an effect similar to that of replacing La by, say, Ce. Detailed analysis on this problem will be presented elsewhere. Also, it would be interesting to experimentally investigate $LnFeAs_{1-y}P_yO_{1-x}H_x$ other than $Ln=Sm$ [22] as another test for the present conclusion. A surprisingly interesting feature of the iron-based superconductors is that the prioritized diagonal motion in the d_{xy} orbitals and the nesting within d_{xy} or $d_{xz/yz}$ Fermi surfaces can all be driving forces of the $s\pm$ -wave superconductivity. This coherent cooperation among various components is indeed the unparalleled identity of the iron-based superconductors.

We thank H. Sakakibara, S. Onari, Y. Yamakawa, and R. Arita for valuable discussions. Numerical calculations were performed at the facilities of the Supercomputer Center, Institute for Solid State Physics, University of Tokyo. This study has been supported by Grants-in-Aid for Scientific Research No. 24340079 and No. 25009605 from the Japan Society for the Promotion of Science. The part of the research at the Tokyo Institute of Technology was supported by the JSPS FIRST Program.

-
- [1] Y. Kamihara, T. Watanabe, M. Hirano, and H. Hosono, *J. Am. Chem. Soc.* **130**, 3296 (2008).
 - [2] I. I. Mazin, D. J. Singh, M. D. Johannes, and M. H. Du, *Phys. Rev. Lett.* **101**, 057003 (2008).
 - [3] K. Kuroki, S. Onari, R. Arita, H. Usui, Y. Tanaka, H. Kontani, and H. Aoki, *Phys. Rev. Lett.* **101**, 087004 (2008).
 - [4] A. V. Chubukov, D. V. Efremov, and I. Eremin, *Phys. Rev. B* **78**, 134512 (2008).
 - [5] S. Graser, T. A. Maier, P. J. Hirschfeld, and D. J. Scalapino, *New. J. Phys.* **11**, 025016 (2009).
 - [6] H. Ikeda, R. Arita, and J. Kuneš, *Phys. Rev. B* **81**, 054502 (2010).
 - [7] M. Daghofer, A. Moreo, J. A. Riera, E. Arrigoni, D. J. Scalapino, and E. Dagotto, *Phys. Rev. Lett.* **101**, 237004 (2008).
 - [8] R. Thomale, C. Platt, W. Hanke, and B. A. Bernevig, *Phys. Rev. Lett.* **106**, 187003 (2011).
 - [9] F. Wang, H. Zhai, Y. Ran, A. Vishwanath, and D. -H. Lee, *Phys. Rev. Lett.* **102**, 047005 (2009).
 - [10] J. Guo, S. Jin, G. Wang, S. Wang, K. Zhu, T. Zhou, M. He, and X. Chen, *Phys. Rev. B* **82**, 180520 (2010).
 - [11] T. Qian, X.-P. Wang, W.-C. Jin, P. Zhang, P. Richard, G. Xu, X. Dai, Z. Fang, J.-G. Guo, X.-L. Chen, and H. Ding, *Phys. Rev. Lett.* **106**, 187001 (2011).
 - [12] Q. Y. Wang *et al.*, *Chin. Phys. Lett.* **29**, 037402 (2012).
 - [13] S. Tan *et al.*, *Nat. Mater.* **12**, 634 (2013).
 - [14] S. Iimura, S. Matsuishi, H. Sato, T. Hanna, Y. Muraba, S. W. Kim, J. E. Kim, M. Takata and H. Hosono, *Nat. Commun.* **3**, 943 (2012).
 - [15] See Supplemental Material, which includes Refs. [16–21].
 - [16] J. P. Perdew, A. Ruzsinszky, G. I. Csonka, O. A. Vydrov, G. E. Scuseria, L. A. Constantin, X. Zhou, and K. Burke, *Phys. Rev. Lett.* **100**, 136406 (2008).
 - [17] N. Marzari and D. Vanderbilt, *Phys. Rev. B* **56**, 12847 (1997); I. Souza, N. Marzari, and D. Vanderbilt, *Phys. Rev. B* **65**, 035109 (2001).
 - [18] T. Miyake, K. Nakamura, R. Arita, and M. Imada, *J. Phys. Soc. Jpn.* **79**, 044705 (2010).
 - [19] H. Usui and K. Kuroki, *Phys. Rev. B* **84**, 024505 (2011).
 - [20] O. K. Andersen, and L. Boeri, *Ann. Phys. (Berlin)* **523**, 8 (2011).
 - [21] H. Usui, K. Suzuki, and K. Kuroki, *Supercond. Sci. Technol.* **25**, 084004 (2012).
 - [22] S. Matsuishi, T. Maruyama, S. Iimura, and H. Hosono, *Phys. Rev. B* **89**, 094510 (2014).
 - [23] G. Kresse, and J. Hafner, *Phys. Rev. B* **47**, 558 (1993); G. Kresse and D. Joubert, *Phys. Rev. B* **59**, 1758 (1999).
 - [24] C. H. Lee, A. Iyo, H. Eisaki, H. Kito, M. T. Fernandez-Diaz, T. Ito, K. Kihou, H. Matsuhata, M. Braden, and K. Yamada, *J. Phys. Soc. Jpn.* **77**, 083704 (2008).
 - [25] A. A. Mostofi, J. R. Yates, N. Marzari, I. Souza, and D. Vanderbilt, (<http://www.wannier.org/>).
 - [26] K. Kuroki, H. Usui, S. Onari, R. Arita, and H. Aoki, *Phys. Rev. B* **79**, 224511 (2009).
 - [27] Y. Yamakawa, S. Onari, H. Kontani, N. Fujiwara, S. Iimura, and H. Hosono, *Phys. Rev. B* **88**, 041106 (2013).
 - [28] K. Suzuki, H. Usui, K. Kuroki, S. Iimura, Y. Sato, S. Matsuishi, and H. Hosono, *J. Phys. Soc. Jpn.* **82**, 083702 (2013).
 - [29] N. E. Bickers, D. J. Scalapino, and S. R. White, *Phys. Rev. Lett.* **62**, 961 (1989).
 - [30] T. Dahm and L. Tewordt, *Phys. Rev. Lett.* **74**, 793 (1995).
 - [31] The actual calculation is done with the orbital basis that are rotated by 45° from the Fe-Fe direction x and y , namely, X and Y defined in Ref. 3. Here, the YZ component of the intraorbital spin susceptibility is adopted.
 - [32] S. Iimura, S. Matsuishi, M. Miyakawa, T. Taniguchi, K. Suzuki, H. Usui, K. Kuroki, R. Kajimoto, M. Nakamura, Y. Inamura, K. Ikeuchi, S. Ji, and H. Hosono, *Phys. Rev. B* **88**, 060501 (2013).
 - [33] T. Miyake, T. Kosugi, S. Ishibashi, and K. Terakura, *J. Phys. Soc. Jpn.* **79**, 123713 (2010).
 - [34] Z.P. Yin, K. Haule, and G. Kotliar, *Nat. Mater.* **10**, 932 (2011).
 - [35] Q. Si and E. Abrahams, *Phys. Rev. Lett.* **101**, 076401 (2008).
 - [36] K. Seo, B. A. Bernevig, and J. Hu, *Phys. Rev. Lett.* **101**, 206404 (2008).

Model of the Electronic Structure of Electron-Doped Iron-Based Superconductors: Evidence for Enhanced Spin Fluctuations by Diagonal Electron Hopping

Katsuhiro Suzuki¹, Hidetomo Usui¹, Soshi Iimura³, Yoshiyasu Sato³,

Satoru Matsuishi⁴, Hideo Hosono^{3,5}, and Kazuhiko Kuroki¹

¹ Department of Physics, Osaka University, Toyonaka, Osaka 560-0043, Japan

³ Materials and Structures Laboratory, Tokyo Institute of Technology, Yokohama 226-8503, Japan

⁴ Materials Research Center for Element Strategy,

Tokyo Institute of Technology, Yokohama 226-8503, Japan and

⁵ Frontier Research Center, Tokyo Institute of Technology, Yokohama 226-8503, Japan

(Dated: November 6, 2018)

I. METHOD

Here we describe the details of the adopted method. In the actual materials, the bond angle reduction occurs almost linearly with doping as shown as α_{La} and α_{Sm} in Fig. S1. In our calculation, we vary the bond angle linearly according to x as $\alpha(x) = -7.48x + 114.36 + \Delta\alpha$, where $\Delta\alpha$ is the amount of parallel shift made with respect to the bond angle variance of the actual La1111.

First principles band calculation is performed by using the VASP package¹. We consider hypothetical materials $\text{LaFeAsO}_{1-x}\text{F}_x$, where the As-Fe-As bond angle is determined as mentioned in the main text. Values of all the other lattice parameters are those determined experimentally for $\text{LaFeAsO}_{0.92}\text{H}_{0.08}$. The effect of partially substituting O by F is taken into account through the virtual crystal approximation. Here, we adopt GGA-PBESol exchange-correlation functional². The wave functions are expanded by plane waves up to cut-off energy of 550eV and 10^3 k -point meshes are used. Five orbital tight-binding models are derived from the first principles band calculation exploiting the maximally localized Wannier orbitals³. The Wannier90 code is used for generating the Wannier orbitals⁴. We neglect the hopping in the z direction and concentrate on the two dimensional model for simplicity.

We consider two sets of electron-electron interactions, orbital independent and dependent ones. In standard notations, the orbital independent interactions are taken as follows : the intraorbital interaction is $U = 1.3\text{eV}$, the interorbital $U' = U - 2J$, Hund's coupling and the pair hoppings $J = J' = U/6$. The orbital dependent interactions are obtained by multiplying a constant factor (0.55 here) to all of the interactions obtained for LaFeAsO in Ref. 5. The results for the orbital independent interactions are shown in the main text, while those for the orbital dependent interactions are shown below.

We apply the FLEX⁶ method to the obtained five orbital model. In FLEX, bubble and ladder type diagrams are collected to calculate the spin $\chi_{ijkl}^S(\mathbf{q}, i\omega_n)$ and charge susceptibilities $\chi_{ijkl}^C(\mathbf{q}, i\omega_n)$, from which the self energy is calculated. Here, i, j, k, l are orbital indices, and the intraorbital susceptibilities displayed in the main text are obtained as $\chi_{iiii}(\mathbf{q}, i\omega_n = 0)$. The renormalized Green function is obtained from the Dyson equation. This pro-

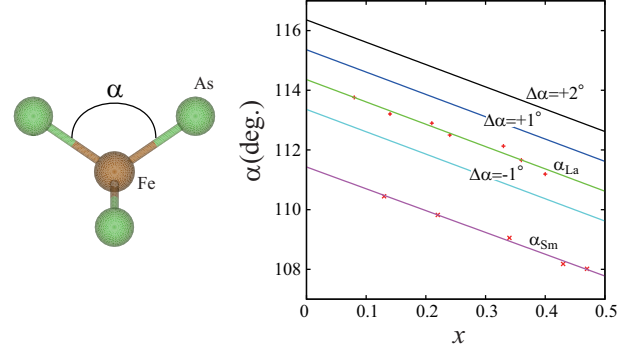


FIG. S1. Doping dependence of the As-Fe-As bond angle. The dots are the actual experimental data.

cess is repeated until a self consistent solution is obtained. As was done in Ref. 7, we subtract the $\omega = 0$ component of the self energy for each iterations, which is considered to be taken into account already in the first principles band calculation. The resulting Green function and the susceptibilities are plugged into the linearized Eliashberg equation, whose eigenvalue λ reaches unity at $T = T_c$, the superconducting transition temperature. Instead of going down to T_c , which is generally a tedious calculation, we obtain λ at a fixed temperature ($T = 0.005\text{eV}$ here), and use it as a qualitative measure for T_c . In the FLEX calculation, we take 32×32 k -point meshes and 4096 Matsubara frequencies. We also perform calculations for 64×64 k -point meshes, or 8192 Matsubara frequencies for comparison for some of the parameter sets.

II. BAND STRUCTURE VARIATION WITH DOPING

The band structure varies with doping as shown in Fig. S2, which is mainly due to the reduction of t_1 . One effect is that the d_{xy} portion around (π, π) is pushed up, which cancels out with the increase of the electron number to result in an unchanged Fermi surface. Another variation with doping occurs around the wave vector $(\pi, 0)$. For small doping rate (large t_1), a saddle point is present in the d_{xy} band around the wave vector $(\pi, 0)/(0, \pi)$, which gives a diverging density of states.

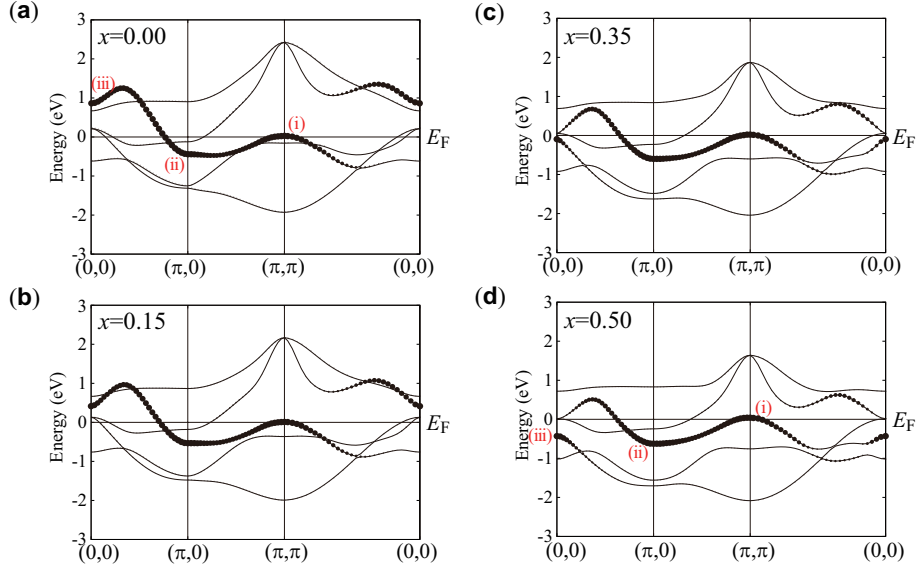


FIG. S2. Band structure variance against doping for $\Delta\alpha = 0^\circ$. (a) $x = 0.0$, (b) $x = 0.15$, (c) $x = 0.35$, (d) $x = 0.5$. The thickness represents the strength of the d_{xy} orbital character. The d_{xy} portion of the band around (π, π) , $(\pi, 0)$, and $(0, 0)$ are denoted as (i), (ii), and (iii), respectively.

Although this van Hove singularity itself is somewhat away from the Fermi level, it does affect the spin susceptibility, which is obtained by summing up contributions including those away from the Fermi level. This kind of band shape is reminiscent of the high T_c cuprates, where the spin fluctuation is enhanced around (π, π) . On the other hand, the saddle point disappears (actually it moves away from $(\pi, 0)$) for small t_1 , and becomes a local minimum. Such a band shape no longer enhances the (π, π) spin fluctuation, and therefore has better matching with the Fermi surface configuration with holes and electrons around (π, π) and $(\pi, 0)/(0, \pi)$, respectively, which itself is in favor of the $(\pi, 0)$ spin fluctuations. Since x_c for $\Delta\alpha = -1$ is smaller than for $\Delta\alpha = +1$, the difference between $\sim (\pi, 0)$ and (π, π) spin fluctuations grows faster with doping for $\Delta\alpha = -1$, as seen in Fig. 4 of main text. The present analysis shows the importance of the prioritized diagonal motion of the electrons for the enhanced $\sim (\pi, 0)$ spin fluctuation and thus $s\pm$ superconductivity.

III. ADDITIONAL ANALYSIS REGARDING THE EIGENVALUE OF THE ELIASHBERG EQUATION AND THE SPIN FLUCTUATION

We show in Fig. S3 the doping dependence of λ obtained by adopting orbital dependent electron-electron interactions proportional to those evaluated in Ref. 5 for LaFeAsO. It can be seen that the overall trend is the same as in the case for the orbital independent interactions presented in the main text.

In the main text, we have not put much focus on the variance of λ against $\Delta\alpha$ (corresponding to the rare earth element dependence of T_c) for a fixed doping rate. As

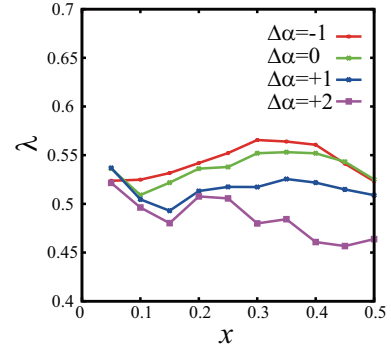


FIG. S3. Eigenvalue of the Eliashberg equation against doping for orbital dependent electron-electron interactions.

seen in Fig.2 of the main text (and also partially Fig. S3 here), λ first increases with decreasing $\Delta\alpha$, then tends to saturate, and finally is reduced for smaller $\Delta\alpha$. This is similar to the trend observed experimentally⁸ as well as the results obtained in a previous theoretical study⁹. In Ref. 9, the reduction of the number of hole Fermi surfaces in the small $\Delta\alpha$ regime has been proposed as the origin of the T_c suppression there, but the more detailed present analysis shows that the λ suppression occurs even when the Fermi surface multiplicity is maximized. Within the present study, the maximum λ is attained when the (π, π) d_{xy} band is touching the Fermi level, i.e., when the d_{xy} Fermi surface nesting appears to be ill-conditioned. In addition to $t_2 > t_1$, this condition also has to be fulfilled for the highest T_c . This is probably because the finite energy spin fluctuation that is responsible for pairing is enhanced when the top of the d_{xy} hole band is touching

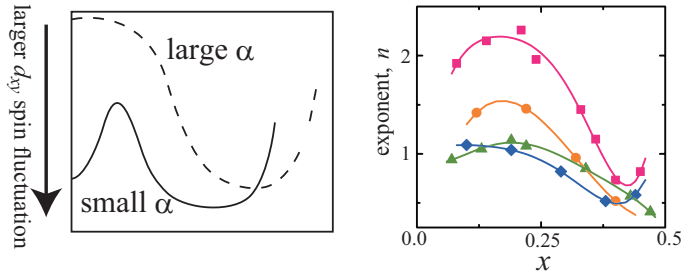


FIG. S4. Left panel : a figure obtained by turning upside down the upper panel of Fig.5 in the main text. Right panel : the experimentally observed doping dependence of the n , where n is the exponent of the temperature dependence of the resistivity $\rho \sim T^n$ (taken from Ref. 10).

the Fermi level. More detailed analysis on this issue is underway.

Regarding the doping dependence of the spin fluctuation, it is interesting to note that if we turn up side down the d_{xy} orbital curves in Fig. S4, they are reminiscent of the n vs. x relation observed experimentally (right panel of Fig. S4)¹⁰, where n is the exponent of the temperature dependence of the resistivity. This means that the exponent is probing the strength of the spin fluctuation within the d_{xy} orbital. This is natural since the portion of the Fermi surface with light mass determines the transport properties, and the light portion (the portion with large group velocity) is indeed the d_{xy} orbital part of the electron Fermi surface.

IV. RE-ENHANCEMENT OF THE d_{xz}/d_{yz} SPIN FLUCTUATION

In addition to the re-enhancement of the d_{xy} spin fluctuation, the d_{xz}/d_{yz} spin fluctuation is also re-enhanced in a even more heavily doped regime as shown in Fig. S5(a). This can again be traced back to the band structure variance with doping. The d_{xy} portion of the band around $(0,0)$ above the Fermi level comes down with doping, and eventually sinks below the d_{xz}/d_{yz} bands, as shown in Fig. S2 (a)~(d). This is once again due to the reduction of t_1 . A band structure reconstruction occurs, and one of the d_{xz}/d_{yz} bands changes into a concave dispersion as shown schematically in Fig. S5 (b)^{11–13}. Therefore, the density of states just above the Fermi level (the hole density of states) increases, thereby enhancing the electron-hole interaction between $\sim (0,0)$ and $\sim (\pi,0)$. Reflecting this re-enhancement of the d_{xz}/d_{yz} spin fluctuations, there appears a “kink” in the λ vs. x plot in the heavily doped regime of $x = 0.35 \sim 0.45$ (Fig.2 of the main text). It should be noted, however, that this effect may be somewhat obscured in the actual materials due to the three dimensionality of the system, which is neglected here.

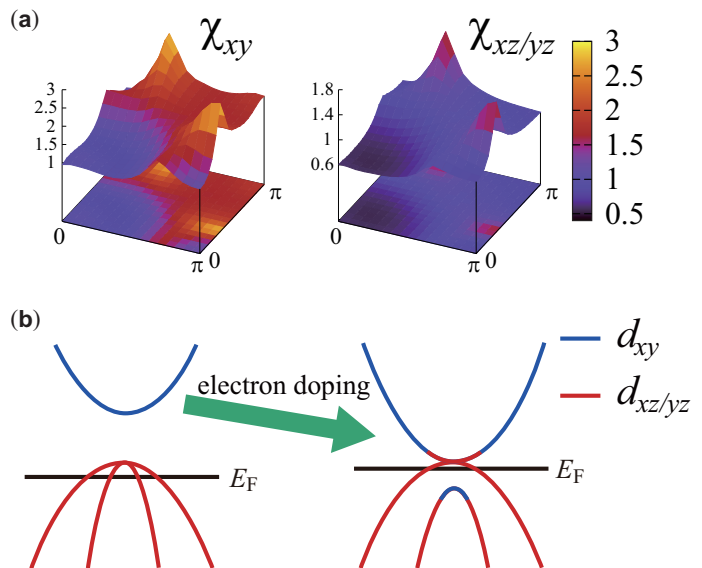


FIG. S5. (a) Intraorbital spin susceptibilities χ_{xy} and $\chi_{xz/yz}$ for $x = 0.35$, $\Delta\alpha = -1^\circ$ (b) schematic figure of the band structure variance around $(0,0)$ with doping.

Namely, this band structure reconstruction actually occurs at k_z that varies with the doping rate^{11–13}.

V. CORRESPONDENCE BETWEEN REAL AND MOMENTUM SPACES

In the cuprates, it is known that the nearest neighbor hopping t_1 dominates. This is likely to favor nearest neighbor pairing in real space, but there are two forms of nearest neighbor singlet pairing, the $d_{x^2-y^2}$ and the extended s -wave pairings. The former and the latter have sign reversing and conserving pair wave functions in real space, which corresponds to the gap forms $\cos(k_x) - \cos(k_y)$ and $\cos(k_x) + \cos(k_y)$, respectively, in momentum space. In the case of the cuprates, the density of states is large around the wave vector $(\pi, 0)$ and $(0, \pi)$, and this is in favor of the $d_{x^2-y^2}$ -wave pairing, whose gap is large around those wave vectors. On the other hand, systems with $t_2 \gg t_1$ can be considered as similar to the cuprates, but with a doubled unit cell, if we neglect t_1 . In momentum space, this gives the gap of the form $\sin(k_x) \sin(k_y)$, namely the d_{xy} -wave pairing, if the density of states is large around the wave vectors $(\pm\pi/2, \pm\pi/2)$, which corresponds to $(\pi, 0)/(0, \pi)$ in the halved Brillouin zone (dash dotted line). In real space, d_{xy} pairing is a next nearest neighbor pairing whose wave function changes sign with 90 degrees rotation. Our present study have revealed that high T_c iron-based superconductors tend to have large t_2 , but there are no Fermi surfaces around $(\pm\pi/2, \pm\pi/2)$, which is unfavorable for d_{xy} pairing. Instead they have Fermi surfaces (or bands near the Fermi level) around $(0, 0)$, $(\pi, 0)$, $(0, \pi)$, (π, π) , which are the points shifted by $(\pm\pi/2, \pm\pi/2)$ from

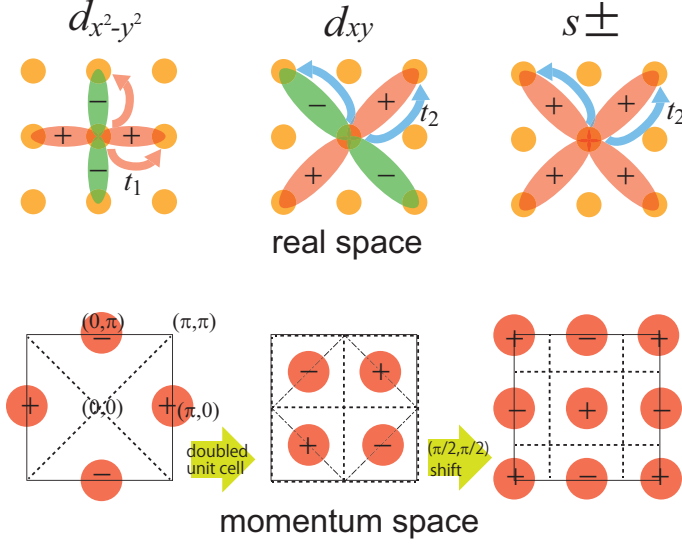


FIG. S6. Correspondence of pairing in real (upper) and momentum (lower) spaces. The signs in the upper panels represent the sign of the pair wave function. The circled areas in the lower panels are those where the density of states near the Fermi energy is large.

the wave vectors $(\pm\pi/2, \pm\pi/2)$. The $(\pm\pi/2, \pm\pi/2)$ shift transforms the d_{xy} gap into $\sin(k_x - \pi/2) \sin(k_y - \pi/2) = \cos(k_x) \cos(k_y)$, i.e., the s_{\pm} form. This gap corresponds to next nearest neighbor pairing in real space, which goes hand in hand with large t_2 , but in a sign conserving form. This relation is schematically depicted in Fig. S6.

-
- ¹ G. Kresse, and J. Hafner, Phys. Rev. B **47**, 558 (1993); G. Kresse, and D. Joubert, Phys. Rev. B **59**, 1758 (1999).
 - ² J. P. Perdew, A. Ruzsinszky, G. I. Csonka, O. A. Vydrov, G. E. Scuseria, L. A. Constantin, X. Zhou, and K. Burke, Phys. Rev. Lett. **100**, 136406 (2008).
 - ³ N. Marzari, and D. Vanderbilt, Phys. Rev. B **56**, 12847 (1997); I. Souza, N. Marzari, and D. Vanderbilt, Phys. Rev. B **65**, 035109 (2001).
 - ⁴ A. A. Mostofi, J. R. Yates, N. Marzari, I. Souza, and D. Vanderbilt, (<http://www.wannier.org/>).
 - ⁵ T. Miyake, K. Nakamura, R. Arita, and M. Imada, J. Phys. Soc. Jpn. **79**, 044705 (2010).
 - ⁶ N. E. Bickers, D. J. Scalapino, and S. R. White, Phys. Rev. Lett. **62**, 961 (1989).
 - ⁷ H. Ikeda, R. Arita, and J. Kuneš, Phys. Rev. B **81**, 054502 (2010).
 - ⁸ C. H. Lee, A. Iyo, H. Eisaki, H. Kito, M. T. Fernandez-Diaz, T. Ito, K. Kihou, H. Matsuhata, M. Braden, and K. Yamada, J. Phys. Soc. Jpn. **77**, 083704 (2008).
 - ⁹ H. Usui, and K. Kuroki, Phys. Rev. B **84**, 024505 (2011).
 - ¹⁰ S. Iimura, S. Matsuishi, H. Sato, T. Hanna, Y. Muraba, S. W. Kim, J. E. Kim, M. Takata and H. Hosono, Nat. Commun. **3**, 943 (2012).
 - ¹¹ T. Miyake, T. Kosugi, S. Ishibashi, and K. Terakura, J. Phys. Soc. Jpn. **79**, 123713 (2010).
 - ¹² O. K. Andersen, and L. Boeri, Ann. Phys. (Berlin) **523**, 8 (2011).
 - ¹³ H. Usui, K. Suzuki, and K. Kuroki, Supercond. Sci. Technol. **25**, 084004 (2012).